Title
Semi-permeable Diffusion Barriers Enhance Patterning Robustness in the C. elegans Germline

Journal
Developmental Cell, 35(4)

ISSN
1534-5807

Authors
Cinquin, Amanda
Zheng, Likun
Taylor, Pete H
et al.

Publication Date
2015-11-01

DOI
10.1016/j.devcel.2015.10.027

Peer reviewed

HHS Public Access

Author manuscript

Dev Cell. Author manuscript; available in PMC 2016 November 23.

Published in final edited form as:

Dev Cell. 2015 November 23; 35(4): 405–417. doi:10.1016/j.devcel.2015.10.027.

Semi-permeable diffusion barriers enhance patterning robustness in the *C. elegans* germ line

Amanda Cinquin[1,3], **Likun Zheng**[2,3], **Pete H. Taylor**[1,3], **Adrian Paz**[1,3], **Lei Zhang**[2,3,4], **Michael Chiang**[1,3], **Joshua J. Snow**[5], **Qing Nie**[2,3], and **Olivier Cinquin**[1,3]

[1]Department of Developmental & Cell Biology, University of California at Irvine

[2]Department of Mathematics, University of California at Irvine

[3]Center for Complex Biological Systems, University of California at Irvine

[5]Department of Biochemistry, University of Wisconsin at Madison; present address: Mirus Bio, Madison WI

Summary

Positional information derived from local morphogen concentration plays an important role in patterning. A key question is how morphogen diffusion and gene expression regulation shape positional information into an appropriate profile with suitably low noise. We address this question using a model system — the *C. elegans* germ line — whose regulatory network has been well characterized genetically but whose spatiotemporal dynamics are poorly understood. We show that diffusion within the germline syncytium is a critical control of stem cell differentiation, and that semi-permeable diffusion barriers present at key locations make it possible — in combination with a feedback loop in the germline regulatory network — for mitotic zone size to be robust against spatial noise in Notch signaling. Spatial averaging within compartments defined by diffusion barriers is an advantageous patterning strategy, which attenuates noise while still allowing for sharp transitions between compartments. This strategy could apply to other organs.

Introduction

Long-range diffusion of signaling molecules is a well-established general mechanism of pattern formation and size control (Wolpert, 1996). If a morphogen diffuses away from a localized source, cells can in principle map their distance to the source by reading the local morphogen concentration: the lower the local concentration read by the cell, the larger the distance to the source. But under this apparently-simple principle lies a fundamental robustness problem (reviewed by Lander, 2011; 2013). The precision of gradients and the molecular machinery cells use to decode them are sharply limited, in part because of

Contact:olivier.cinquin@uci.edu.

[4]Present address: Beijing International Center for Mathematical Research, Center for Quantitative Biology, Peking University, Beijing, China

molecular noise. Readouts of low morphogen concentrations may thus be particularly noisy, and fluctuations in intensity or location of the morphogen source could lead to errors in positional information estimated from morphogen concentration away from the source. How tissues are robustly patterned despite molecular noise is thus a question of outstanding interest.

Consistent with the idea that robustness of positional information is an important design principle of developing organisms, morphogen gradients are as a rule not simply generated by free extracellular diffusion but are in addition actively shaped by the tissues they are patterning. Two broad classes of mechanisms have been well studied by which diffusion of morphogens is controlled to shape their gradient. In a class of mechanisms active throughout the tissue, morphogens physically interact with coreceptors and extracellular matrix proteins that are thought to control local diffusion (e.g. Yan et al., 2010); the very interaction between morphogen and receptors that read their concentration can also be used to shape the gradient in a desirable way (Eldar et al., 2003; Lander et al., 2009). In a mechanism active at specific positions in the tissue, barriers can block morphogen diffusion across boundaries between morphogenetic subunits, thus allowing these subunits to be patterned independently (Rinne and van der Schoot, 1998; Kornberg and Guha, 2007). A less explored third possibility is that diffusion barriers could be only *semi*-permeable and used not to set the boundaries of a domain reachable by a diffusing morphogen molecule, but to shape the overall spatial profile by slowing down morphogen diffusion at key points. The relevance of such a mechanism is supported by the role of cellular structures in shaping the Bicoid gradient in the *Drosophila* embryo (Coppey et al., 2007; Kavousanakis et al., 2010; Daniels et al., 2012).

The *C. elegans* hermaphrodite gonad is a well-established model system for patterning and stem cell differentiation (Hubbard and Greenstein, 2005; Kimble and Crittenden, 2007; Hansen and Schedl, 2013), in which diffusion can be readily assayed experimentally. The hermaphrodite gonadal arm forms a tube; stem cells reside at the distal end within a “mitotic zone” (MZ; Figure 1A), and cells progressively differentiate as they are displaced from that end in a proximal direction — initially entering the ‘transition zone” (TZ). GLP-1/Notch signaling provided by the “Distal Tip Cell” (DTC) — which forms the stem cell niche — is required for stem cell self-renewal and is known to provide a major source of positional information (Kimble, 1981; Kimble and White, 1981; Austin and Kimble, 1987). But while the control of proliferation and differentiation in the MZ has been extensively characterized at the genetic and biochemical levels (see Figure 1B for core regulatory network downstream of GLP-1/Notch), a physical feature that could play a key role in long-range patterning and local cell coordination has received limited attention: germ “cells” form a syncytium, where nuclei are enclosed by partial plasma membrane that has large openings on a central cytoplasmic core called the “rachis” (Abi-Rached and Brun, 1975; the rachis is spanned in various places by small sets of nuclei that form bridges, Hirsh et al., 1976; Hall et al., 1999; Amini et al., 2014). This physical structure could allow regulatory products to readily diffuse from one cell to another, thereby leading to extensive crosstalk between cells. The role of such syncytial diffusion in controlling pattern formation and germline stem cell differentiation has been virtually unstudied.

Results

Semi-permeable barriers shape diffusion gradients

To verify that long-range diffusion takes place within the germline syncytium, we injected fluorescent molecules of different composition and size in the proximal region of gonad arms, and assayed distal diffusion (Figure 1A). Fluorescein (molecular weight of ~0.3 kDa) diffused quickly, as expected given its small size; fluorescein had spread to the distal end by the time samples were mounted for imaging (Figure 2A). To ask whether larger molecules could also undergo long-range diffusion, we injected EGFP (molecular weight of ~30 kDa) and a 10 kDa fluorescently-labeled dextran. Injected molecules also diffused all the way to the distal end (Figure 2B–C; a lag was noticeable before distal fluorescence was detected). Long-range diffusion thus readily takes place in the *C. elegans* germline syncytium.

To further characterize the diffusion of molecules within the gonadal arm, we examined spatial concentration profiles of injected EGFP or 10 kDa dextran. We found steps in the fluorescence intensity profiles (Figure 2B–C); such steps could in principle be formed by local restrictions to diffusion, or by enhanced degradation or extrusion of injected molecules in the distal region. To distinguish between these possibilities, we injected labeled molecules at the distal end of the gonad. We found a reversed intensity profile, with a distal to proximal decrease in fluorescence intensity that also showed steps (Figure 2D). We thus conclude that the germline syncytium contains barriers that slow down but do not completely block diffusion.

Local rachis constrictions are sufficient to create steps

We next started querying the physical nature of the diffusion barriers. Steps in dextran intensity colocalized with cell bridges spanning the rachis (Figure 2E). To further assay the relationship between dextran steps and cell bridges, we injected dextran in a strain expressing the membrane marker *NMY-2::GFP*; we observed that steps in dextran intensity colocalized with the plasma membrane of cells belonging to bridges (Figure 2F–I). This indicates that diffusion barriers are associated with cell bridges spanning the rachis, and are formed at least in part by plasma membrane belonging to bridge cells. To ask how cell bridges could impede diffusion through the rachis, we performed three-dimensional reconstructions of the rachis and observed that cell bridges cause a local constriction in the rachis (Figure 2J–M); the order of magnitude of local diameter at the restriction is 1 μm. Other than this constriction, we did not identify any other structures such as lipid bilayers that could impede diffusion.

To test whether rachis constrictions could be sufficient to create effective diffusion barriers, we measured diffusion coefficients and turned to mathematical modeling. We measured the diffusion coefficient of injected 10 kDa dextran using single-point fluorescence correlation spectroscopy (Ries and Schwille, 2012). A fit to Fick's second law yielded a diffusion coefficient of ~20 $\mu m^2.s^{-1}$. We built a mathematical model based on a simple two-dimensional geometry for the rachis inspired from experimental observations, and assayed time evolution of the dextran concentration after simulated injection in the proximal region (see Data S1; the model did not incorporate an advection term because the rate of cell

movement along the distal proximal axis of ~1 row per hour, Crittenden et al., 2006, translates to at most ~5 μm per hour and is thus negligible compared to the diffusion rate). Steps in simulated dextran intensities of magnitude commensurate with experimental data persisted for ~1 hour (Figure 2N–O), before diffusion equalized the concentrations over the distal-proximal axis. This suggests that the rachis constrictions are sufficient to create diffusion barriers despite their diameter being much larger than that of individual protein molecules.

Diffusion barriers colocalize with key positions of cell state change

To begin addressing the functional role of diffusion barriers, we examined the relationship between positions of the barriers and the positions at which differentiation steps occur. Steps in expression of the differentiation marker GLD-1 (Francis et al., 1995a; 1995b) are detectable along the distal proximal axis as previously reported (Cinquin et al., 2010), using a GLD-1::GFP reporter (Schumacher et al., 2005). In all cases we examined, these steps colocalized with distal diffusion barriers revealed by dextran injection (n = 41 injected *gld-1::gfp* worms with otherwise wildtype background; Figure 2P; n = 71 injected *gld-1::gfp* worms with non wildtype backgrounds). Consistent with our analysis of dextran-injected worms, GLD-1 steps are only found at positions where a cell bridge spans the rachis (n > 200; Figure 2P). We further observed that the positions of GLD-1 steps within the MZ cluster at rows 7–8 and 11–12 (Figure 3A; rows are counted in cell diameters from the distal end). Rows 7–8 are the approximate position of the boundary between distal and proximal pools of germ cells that were found to be dissimilar in their differentiation properties (Cinquin et al., 2010). Rows 11–12 could correspond to the position beyond which a number of cells have entered premeiotic S phase (Fox et al., 2011). In addition, there is a barrier at the MZ/TZ transition (Figure 3B; this more proximal barrier is not associated with a GLD-1 step). We conclude that diffusion barriers occur at positions where germ cells are transitioning through differentiation states.

Long-range diffusion controls behavior of both distal and proximal MZ cells

We next asked whether the role of diffusion barriers might not be limited to defining interfaces between MZ compartments, but could also include control of MZ size as a whole. We found significant correlation between position of GLD-1 steps and size of the MZ (Figure 3C; step 1: $R^2 = 0.4$, $p < 0.001$; step 2: $R^2 = 0.5$, $p < 0.002$). This correlation shows that the size of the MZ could be controlled by diffusion barrier position, that diffusion barrier position could be controlled by MZ size, or that both could be downstream of a third control. To begin distinguishing between these possibilities, we created artificial barriers by injection of oil droplets within the syncytium (Nadarajan et al., 2009). We validated the effect of droplet injection by targeting the pachytene region, which contains no detectable endogenous barriers — this minimizes the risk of confusion between the effects of endogenous barriers and of oil droplets. Oil droplets significantly slowed down but did not completely block diffusion of injected dextran (Figure 3D), similar to endogenous barriers. MZ size was reduced 18 hr after distal oil droplet injection compared to control water injection (n = 10 for each, p < 2.3E-5; Figure 3E–F). Although it remains possible that presence of oil creates a local stress that contributes to MZ size change, and although some nuclei close to the droplet take a condensed appearance of unclear significance (Figure S1),

water-injected controls show that the injection process itself does not create a local or global response responsible for MZ size change. Furthermore, oil-injected gonads maintain a number of M-phase cells similar to controls (Figure S1), suggesting continued cell cycling at a normal rate. It is also possible that presence of oil droplets impedes normal cell movement, but droplets do not fully obstruct the gonadal arm (Figures 3 and S1), they are possibly displaced along the distal-proximal axis as in the proximal gonad (Wolke et al., 2007), and their presence does not lead to accumulation of distal cells despite maintenance of mitotic cells (Figure S1); since in addition there is strong correlation between droplet position and MZ end, we conclude that impeded cell movement is unlikely to have a major contribution to our results. The strength of the correlation between MZ size and artificial barrier position was similar to that between MZ size and first endogenous barrier position ($R^2 = 0.5$, $p < 0.01$ and $R^2 = 0.4$, $p < 0.03$ respectively; Figure 3G). We thus conclude that the endogenous diffusion barriers likely play a role in MZ size control.

To further assay the role of diffusion barriers in control of MZ size, we next asked if diffusion barriers have a role in regulating differentiation of the distal and/or proximal MZ pools that we identified earlier (Cinquin et al., 2010). We previously reported that distal MZ cells do not differentiate when *emb-30(tn377ts)* mutants are shifted to the restrictive temperature, causing loss of anaphase promoting complex activity and M-phase accumulation. Proximal MZ cells do differentiate, and a sharp GLD-1 border forms between the two regions. We injected a fluorescently-labeled dextran in *gld-1::gfp; emb-30* mutants shifted to the restrictive temperature for 9–12 hr (Figure 4B). At the border between differentiated and undifferentiated cells, we found a diffusion barrier that is less permeable than in controls (Figure 4A): no dextran diffusion into the distal region was detected (Figure 4B; n = 15/15). This enhanced diffusion barrier colocalized with a layer of F-actin that separated distal and proximal regions (Figure 4C). Upon upshift of *emb-30*, the distal MZ is thus sealed off from the rest of the gonad by a diffusion barrier unlike those seen in wild type.

The presence of a particularly tight diffusion barrier in upshifted *emb-30* raises the possibility that the contrasting differentiation responses of distal and proximal MZ pools are due to changes in regulator diffusion, rather than to intrinsic characteristics of distal and proximal cells. To further explore this idea, we turned to *C. elegans* males. The male MZ does not contain cell bridges (Morgan et al., 2010), and has an open rachis that extends to the distal end (Figure 4D,F). We could not identify diffusion barriers by dextran injection into upshifted *gld-1::gfp* (n = 6; Figure 4D) or unshifted *gld-1::gfp; emb-30* males (n = 5). By contrast, a diffusion barrier appeared in upshifted *gld-1::gfp; emb-30* males (n = 6; Figure 4E), as the rachis distal to the MZ/TZ boundary closed and proximal MZ cells differentiated (Figure 4E,G). Therefore, *emb-30* upshift appears to tighten existing diffusion barriers (in hermaphrodites), or to create them *de novo* (in males). In both cases, the boundary between differentiating and non-differentiating cells precisely colocalizes with the diffusion barrier. We do not know the mechanisms, either direct or indirect, that result in barrier tightening upon *emb-30* removal. In any case, our data suggest that the effect of *emb-30* loss of function on cell differentiation might not be mediated directly by cell cycle

disruption, but perhaps through modulation or creation of diffusion barriers that in turn sharpen or create differences between distal and proximal cells.

Overall, our data strongly support the idea that diffusion barriers play an important role in controlling differentiation behavior of proximal MZ cells. To ask whether this is also true of distal cells, we assayed whether the differentiation behavior of distal cells is affected by artificial barriers. We injected oil within the MZ and assayed whether the artificial barrier created altered the response of distal cells to removal of Notch signaling. We previously reported that upshift of the temperature-sensitive Notch mutant *glp-1(q224)* to 25°C causes differentiation of the distal MZ within 6 hours (Cinquin et al., 2010). To increase the time resolution of our experiments, we repeated this experiment by upshifting to only 20°C; differentiation took 10 hours to complete (Figure 4H). We found that differentiation was preceded by a loss of both GLD-1 steps and diffusion barriers (Figure 4I–L). Crucially, if this loss of diffusion barriers was compensated by the presence of an artificial diffusion barrier in the MZ of one gonadal arm, differentiation of distal cells was blocked in that arm (Figure 4M) whereas in the control arm of the same worm, as well as in water-injected controls, MZs differentiated (Figures 4N–O). Since droplet injection reduces MZ size (Figure 3E–F), droplets appear to selectively block differentiation of cells that are located distal to them. Proximal to distal diffusion of differentiation-promoting factors thus appears necessary for distal cells to differentiate in response to loss of Notch signaling. Conversely, shortening of the MZ in response to oil droplet injection suggests that differentiation of proximal MZ cells is controlled by diffusion of distal factors. Overall, our data thus underscore that both distal and proximal MZ cells behave non-autonomously, and that the distal and proximal zones influence each other through syncytial diffusion.

Weak correlation between MZ size and proximal reach of distal tip cell processes

The best-characterized source of positional information within the MZ is provided by the stem cell niche formed by the DTC, whose nucleus and main cytoplasmic mass are located at the MZ distal end, and by Notch signaling that the DTC induces in stem cells: both are critical for stem cell self-renewal (Austin and Kimble, 1987), sufficient for establishment of a mitotic state, and polarize the MZ (Kimble and White, 1981). Syncytial diffusion of differentiation-controlling Notch targets induced in distal-most germ cells by the DTC thus provides a plausible mechanism by which MZ size could be controlled. However, although the bulk of the contact between DTC and germ cells occurs distally (Crittenden et al., 2006; Byrd et al., 2014) in a “plexus” region whose relationship with MZ size is not fully resolved (Byrd et al., 2014), the DTC also possesses filopodia called “processes” that can extend from the distal end all the way to the proximal end of the MZ (Fitzgerald and Greenwald, 1995 Figure 1A). These processes carry at least one kind of Notch ligand (Crittenden et al., 2006), and a possibility is thus that the end of the MZ could be simply defined by the end of the longest distal process, with a minimal role for diffusion in MZ size control.

The idea that the proximal extent of DTC processes controls MZ size appears to be contradicted by the fact that the longest DTC processes get longer as worms age while the MZ gets shorter (Crittenden et al., 2006). However, it could still be that proximal-most processes do play a major role in extending MZ size, but that an offset develops with age

between MZ boundary and process end (e.g. if MZ length is also controlled by an independent factor that changes with age). To ask more directly if we could detect a major contribution of proximal processes in MZ size control, we tested whether longest DTC process length correlates with MZ size. We found that such a correlation does exist (R^2 = 0.26 at day 1 of adulthood, p < 3.1E-3; Figure S2A), but that it is substantially weaker than the correlation between distal diffusion barrier position and MZ size (R^2 = 0.4–0.5 at day 1 of adulthood, Figure 3C). Furthermore, the correlation between DTC process length and MZ size disappears by day 2 of adulthood (R^2 = 0.01, p > 0.68; Figures S2B–C), while the correlation between barrier position and MZ size is maintained (R^2 = 0.7–0.8, p < 1.5E-2 at day 2 and R^2 = 0.4–0.5, p < 0.02 at day 3; Figures S2D–G). Therefore, DTC processes may play a role in defining the spatial pattern of Notch activation but the proximal extent of the processes appears to play a minimal role in controlling MZ size.

Notch expression is high and noisy in the distal MZ

As a next step in asking how diffusion barriers contribute to patterning of the *C. elegans* gonad, we quantified the spatial expression profile of Notch — the receptor whose activation provides the positional information assumed to underlie that patterning. Despite the central role of Notch in MZ specification and maintenance, the pattern of GLP-1/Notch expression within the MZ had not been characterized. We used a strain expressing a GLP-1/Notch::GFP protein fusion under control of the endogenous *glp-1/Notch* promoter (Sarov et al., 2012). The receptor localizes largely to the plasma membrane (Figure 5A), consistent with previous reports (Crittenden et al., 1994). Quantification showed that membrane expression is high in the distal-most ~11 rows, and decays within the proximal MZ (Figure 5B–C); positions of diffusion barrier clusters (Figure 3A) appear to correspond to inflexion points in the average GLP-1/Notch::GFP profile. Sustained expression of the receptor at high levels up to the average position of the second diffusion barrier, as well as intimate contact between the DTC and germ cells over the first ~8–9 rows (Byrd et al., 2014), strongly suggest that Notch activation extends over a substantial portion of the MZ.

We next asked how much variability is found in Notch membrane expression within and across gonadal arms. On a qualitative level, overall distal-proximal profiles of Notch expression displayed high intra- and inter-gonad variability (Figure 5B–C). To put these observations on a quantitative footing, we relied on the coefficient of variation (CV), which is defined as the ratio of standard deviation to mean and thus provides a unit-free measure of noise. The CV for membrane Notch was high in the distal MZ — ranging from 0.19 over the first ~2 rows to 0.13 for rows ~7–9. This variability comes in addition to high dynamicity and high inter-individual variability of DTC morphology (Wong et al., 2013), and likely results in strong variability of Notch activation. This is in contrast to low variability in MZ size (CV = 0.10, computed from n = 30 gonads). Therefore, mechanisms are likely at play that minimize the sensitivity of MZ length to spatial fluctuations in Notch signaling intensity.

Modeling suggests MZ size control by diffusion barriers

To investigate the expected interplay downstream of Notch signaling between diffusion barriers and MZ size control, we built models considering synthesis and degradation of key

regulatory molecules (Figure 1B), as well as diffusion within a spatial domain accounting for the rachis. In these models, Notch signaling drives transcription of an “FBF” species, which encompasses both FBF-1 and FBF-2 (the FBF genes are collectively necessary for adult germ cell proliferation; *fbf-2* has been suggested to be a direct Notch target; Lamont et al., 2004). FBF represses both its own expression and expression of GLD-1 (Crittenden et al., 2002), which promotes differentiation (Francis et al., 1995b). As a parsimonious assumption, the model defined the position of the border between the MZ and cells in meiosis by a threshold level of 1.0 arbitrary GLD-1 units; a more intricate mechanism involving a combination of FBF and GLD-1 levels is certainly theoretically possible but lacks experimental support. Although in *ad hoc* mutant backgrounds proliferation can occur in the absence of FBF (Crittenden et al., 2002) and transient meiotic entry occurs in the absence of GLD-1 (Francis et al., 1995a), FBF and GLD-1 were the most natural choices for our model because of their central roles highlighted in multiple studies and because of their thorough experimental characterization (Kimble and Crittenden, 2007). Other differentiation factors and other Notch targets (e.g. Schmid et al., 2009; Kershner et al., 2014) could certainly be incorporated in more sophisticated models but that would lead to the models being more poorly constrained, which would make it more difficult to derive general principles. The full mathematical definition of our model, as well as a parameter robustness study, are provided as Data S1.

An important question in defining the models is what mechanisms control position of the diffusion barriers within the MZ. We first considered a model following which the diffusion barriers were fixed at constant positions independent of Notch signaling or FBF or GLD-1 levels. While these models correctly reproduced the GLD-1 and FBF expression patterns on the distal-proximal axis, they displayed a negative correlation between MZ size and the distances from the distal end at which diffusion barriers were placed (Figure 6A–B). This negative correlation, which holds under a variety of conditions, is in contradiction with the positive correlation we observed experimentally.

We thus next considered a model in which the positions of the diffusion barriers were themselves regulated by Notch signaling. The processes by which the barriers form, and how they might move along the distal-proximal axis as a result of cell proliferation are unknown. Given these unknowns, the model we used simply had dynamical updates of barrier positions in the course of the simulation — so that these positions tracked a given GLD-1 level. There was thus feedback between barrier position and GLD-1 levels: barriers shaped the profile of GLD-1 by controlling its diffusion, while GLD-1 set the positions of the barriers. We found that this model correctly reproduced the spatial profile of GLD-1 expression similarly to the earlier model, but that in addition it could place the diffusion barriers at the correct positions and could readily reproduce the positive correlation between barrier position and MZ size observed in experimental data (Figure 6C; Data S1). While we cannot exclude that barrier positions are in fact controlled independently of Notch signaling by an unknown upstream regulator that also influences MZ size, the model we propose provides a fitting and parsimonious explanation of the data.

As a test of our model, we asked whether it could account for differences between male and hermaphrodite MZs. We characterized male and hermaphrodite MZ size robustness against

global perturbation in Notch signaling, using the Notch *q224* temperature-sensitive mutant at a range of semi-permissive and non-permissive temperatures. We found that MZ size is less robustly maintained in males than in hermaphrodites as temperature increases (Figure 6D). One key difference between male and hermaphrodite MZs is the lack of diffusion barriers in the former (Figure 4D). Numerical simulations of our model show that the removal of diffusion barriers lowers robustness against changes in total intensity of Notch signaling (Figure 6E). This supports the relevance of diffusion barriers to MZ size control, and the ability of our model to account for this control.

Diffusion barriers and a negative feedback loop provide robustness against spatial fluctuations in Notch signaling

We next hypothesized that diffusion barriers could also make MZ size robust against variations in the spatial distribution of Notch signaling. To test this idea, we performed numerical simulations of the changes in GLD-1 profiles when the distal profile profile of GLP-1/Notch activation was perturbed in a way that the total signaling intensity was preserved. We found that, while MZ size is sensitive to the sum of Notch activity, both fixed and mobile diffusion barriers make MZ size robust against perturbations that conserve total Notch activity (Figure 6F–K). Diffusion barriers thus appear to have a role of prime importance in making MZ size robust against the spatial noise in Notch signaling that we observed.

Finally, we asked whether an intriguing motif within the regulatory network might play a role in providing patterning robustness. Specifically, FBF self-inhibition is well documented (Lamont et al., 2004) but a role for this self-inhibition has yet to be investigated. We thus performed simulations based on the same model as detailed above, but in which we increased the strength of FBF negative feedback. On one hand, we found that robustness of MZ size to changes in the spatial distribution of Notch signaling was substantially increased (Figure 6J), as long as total signaling intensity was preserved. On the other hand, robustness of MZ size to total Notch signaling intensity was decreased (Figures 6L–M). A combination of strong FBF negative feedback and diffusion barriers thus makes it possible for MZ size to be sensitive to total Notch signaling intensity — which is potentially a highly-relevant control parameter, given that MZ size responds to changes in nutrient availability at least in part through the stem cell niche (Dalfó et al., 2012) — but not to the particulars of the spatial distribution of Notch signaling, which is highly variable. Overall, considering MZ size control as a performance objective thus makes it possible to assign functions to motifs in the germline regulatory network that might otherwise remain obscure.

Discussion

Although a number of mutations have been identified that affect MZ size (e.g. Eckmann et al., 2004; Lamont et al., 2004), the overall mechanisms that control that size are still poorly understood. The proximal end of the DTC does not define the MZ/TZ boundary (Crittenden et al., 2006), nor does it correlate with the position of that boundary — other than at a particular stage of development. We propose that it is the local state of the regulatory network that determines the location at which cells differentiate. At any given spatial

location, this state depends not only on local Notch activation as a result of contact with the DTC, but also on diffusion of Notch targets through the syncytium (and also possibly on diffusion of the Notch intra-cellular domain itself, although that diffusion may be more limited because of sequestration by the nucleus or by other cellular structures). Diffusion barriers appear to play an important, long-range role in determining regulatory network state. These barriers are placed at positions that correspond to important changes in cell behavior; for example, the G2 index increases around row 12 (Chiang et al., 2015), where one barrier is often found, and crescents form around row 20, where another barrier is systematically found. Labeled dextran and oil droplet injections show that presence of the barriers affects cells that are located away from the barriers, a result further supported by simulations showing that MZ size is impacted by barriers found ~mid-way in the MZ. Overall, we propose that the spatial pattern of Notch activation, which likely depends on the extent of the DTC processes, and syncytial diffusion of Notch targets, which is shaped by the diffusion barriers, interact to control MZ size.

It appears that Notch activation at the very distal tip of the MZ, combined with fast distal-proximal diffusion of Notch target protein products, could be sufficient to provide positional information specifying the proximal end of the MZ. Yet the presence of Notch-ligand-carrying DTC processes (Fitzgerald and Greenwald, 1995; Crittenden et al., 2006; McGovern et al., 2009) and expression of Notch receptor across the whole MZ, as well as expression of *fbf-2* (Lamont et al., 2004), *sygl-1*, and *lst-1* (Kershner et al., 2014) further than the distal tip, strongly suggest that Notch activation extends over a substantial portion of the the MZ distal-proximal axis. What might be the advantage of this extended activation? Given the wide array of Notch targets (e.g. Krejcí et al., 2009), one can speculate that Notch controls not only MZ size but also other characteristics such as cell cycling speed, which varies across the distal-proximal axis of the MZ (Chiang et al., 2015). Furthermore, dose-dependent specification of cell fate by Notch has been shown in a number of tissues (Guentchev and McKay, 2006; Ohlstein and Spradling, 2007; Mazzone et al., 2010; Guruharsha et al., 2012). Therefore, the overall pattern within the MZ of activity of Notch and its targets may be just as important as the location at which this activity drops below the threshold defining the MZ/TZ boundary. The DTC extending on the distal-proximal axis makes it possible to create patterns of Notch activity across the distal-proximal axis that may not be achieved by simple diffusion from a punctual source located at the distal end, even if that diffusion is shaped by barriers.

A mechanism whereby Notch activation is distributed along the distal-proximal axis instead of being localized to the very distal end introduces a weakness: MZ size is made sensitive to noise in the spatial extent of Notch activation. This noise is expected to be substantial, given that there is strong variability in membrane Notch expression, and given that the DTC is highly dynamic and variable across individuals (Wong et al., 2013) and does not make contact with all cells. If left unbuffered, the noise in Notch activation might impede progress through differentiation in an orderly fashion. Although diffusion barriers may play an important role in their own right in shaping the Notch activity profile, an additional role may be to provide patterning robustness. We showed that barriers can virtually remove the effect of spatial noise in Notch activation on MZ size, while still allowing total Notch signaling

intensity to control MZ size. In a sense, barriers may thus enable multiplexing of information provided through Notch signaling: they may allow Notch to differentially control cells within the MZ following a particular profile, while allowing MZ size to be controlled by total Notch intensity independently of the particular profile within the MZ. Interestingly, unlike hermaphrodites males do not have large DTC processes and also do not have diffusion barriers. Although it is not clear why hermaphrodite MZs would need to be patterned differently from male MZs, the correlation between existence of DTC processes and existence of diffusion barriers is compatible with the idea that barriers provide robustness against noise in spatial positioning of the DTC.

We note that the regulatory network model on which we relied is certainly simplistic, as is the assumption that the MZ/TZ boundary is defined by a threshold GLD-1 level. Nonetheless, this model has allowed us to identify a potential role for a network motif whose purpose had remained obscure until now. Specifically, we showed that FBF self-repression is important for robustness of MZ size against noise in the profile of Notch activation — and that it also plays in role in controlling sensitivity of MZ size to total Notch activation. It will be interesting to expand the regulatory network models to further study the interaction between features of those models and diffusion in patterning of the MZ, and to explore specific mechanisms by which the network may regulate position of the MZ/TZ and of the diffusion barriers.

How does the *C. elegans* germline compare with other syncytial tissues? A number of tissues other than gonads form syncytia (Gladfelter et al., 2006; Shi et al., 2009). At least one of these syncytia, the vertebrate lens, also possesses diffusion barriers: it is “stratified” in concentric layers with little diffusion from one layer to the other (Shestopalov and Bassnett, 2003; Shi et al., 2009). Although the functional significance of that stratification awaits further study, its presence shows that regulated diffusion is a feature shared by syncytia other than the *C. elegans* germ line.

The syncytium in which the role of diffusion has been most thoroughly studied, the early *Drosophila* embryo, has not been reported to possess large scale diffusion barriers. There are nonetheless three known ways in which this system departs from free diffusion. First, nucleocytoplasmic shuttling of patterning factors reduces their effective diffusion coefficient during interphase (Gregor et al., 2007; Sample and Shvartsman, 2010). Second, membrane furrows that periodically extend into the syncytium play a complementary role in reducing the effective diffusion coefficient during mitosis (Daniels et al., 2012). Third, the secretory system and plasma membrane are “functionally compartmentalized” around nuclei even before cellularization occurs (Frescas et al., 2006; this compartmentalization is different from the one we report, notably in that it does not impede diffusion of injected dextrans, Mavrakis et al., 2009). Each of these three mechanisms lowers the effective speed of long-range diffusion by the presence of local structures (including nuclei and furrows) repeated a number of times throughout the tissue. This is in contrast to the diffusion barriers we report, which are present in at most three locations through mitotic zones.

It has been suggested that spatial averaging resulting from free diffusion in the *Drosophila* embryo syncytium contributes to the robust readout of a morphogen gradient (Gregor et al.,

2007). But simple spatial averaging comes with a significant drawback in that it blurs the spatial pattern at the same time as it suppresses noise. A crucial feature of large-scale diffusion barriers reported here is that they provide a simple way to maintain relatively large domains that have sharp differences in concentrations of morphogens and their readouts, yet can still communicate by controlled diffusion from one domain into the other. Large, distinct domains comprised of a number of cells might be more relevant to later stages of development than to the initial stages of growth.

Importantly, the principle of inter-cellular diffusion of regulatory molecules also extends to cells that do not form syncytia. An increasing number of regulators that were thought to act solely intracellularly are now known to translocate across membranes and to have cell non-autonomous effects. This is the case of homeodomain proteins that play a critical role in patterning the developing nervous system (Brunet et al., 2007), and also intriguingly of the tumor suppressor PTEN (Hopkins et al., 2013). There may be many more such translocating proteins to be discovered, and spatial averaging of the concentrations of many regulators could therefore take place independently of the limited set of specialized inter-cellular signaling pathways. We speculate that yet-to-be-characterized diffusion barriers might play a crucial role in defining the domains over which such averaging occurs, and in minimizing molecular noise within these domains.

Experimental Procedures

Worm strains and maintenance

Strains used were Bristol N2, BS1080: *gld-1::gfp(ozIs5)* (Hansen et al., 2004), JJ1473: *nmy-2::gfp(zuIs45)* (Nance, 2003), DG627: *emb-30(tn377ts)* (Furuta et al., 2000), JK1107: *glp-1(q224ts)* (Austin and Kimble, 1987), and EV343_OP237: *unc-119(ed3)*; [WRM0614A_B09::*unc-119*-Nat([17514] *glp-1*::2xTY1wEGFP 3xflag)] (Sarov et al., 2012). Strains were maintained as described (Brenner, 1974) using *E. coli* HB101 as a food source, at 20°C or at the permissive temperature of 15°C for *glp-1(ts)* and *emb-30(ts)*. Worms were staged by picking L4s based on vulva morphology, and were used 24 hours later unless otherwise specified.

Antibody staining and quantification

Antibody and DNA staining were performed on extruded gonadal arms as described (Crittenden and Kimble, 1999), with a 10-minute, room-temperature 4% PFA fixation step followed by a 15-minute, 0.1% Triton X-100 permeabilization step, a 30-minute, 0.5% BSA blocking step, overnight incubation at 4°C with primary antibodies. Gonads were stained with 1:50 (GLP-1::GFP) or 1:1000 (GLD-1::GFP) anti-GFP antibody (ab5450, Abcam, Cambridge, MA), 1:200 anti-GLD-1 and anti-phosphohistone H3 (2851S, Cell Signaling, Beverly, MA). Secondary antibodies Alexa 488 and 649 were used at 1:200 (A21467, A10524, Invitrogen, Grand Island, NY), Phalloidin at 0.17 μM (Invitrogen, Grand Island, NY, A12379 or A22283), and DAPI at 1 μg/mL DAPI. For anti-GLD-1 staining, 0.1% Triton X-100 was added to antibody solutions. Confocal stacks were acquired at ~0.3 μm intervals using LSM710 or LSM780 microscopes (Carl Zeiss MicroImaging, Oberkochen,

Germany) using a 63x objective, or a FV1000 (Olympus, Center Valley, USA) with 60x objective.

Injections

Worms were mounted in halocarbon oil (H8898, Sigma-Aldrich, St. Louis, MO) on a dried agarose pad. Fluorescent molecules were injected using BF100-87-10 capillaries (Sutter Instruments, Novato, CA) pulled with a P87 needle puller (Sutter Instruments), and a Femtojet injector and Transferman NK2 micromanipulator (Eppendorf, Hamburg, Germany). The site of injection was in the pachytene region unless otherwise stated, at a distance from the distal end of about a third to half of the total distance to the loop region. 10 kDa neutral dextran conjugated to rhodamine B (D1816, Invitrogen, Grand Island, NY) was injected at 0.1 mM, purified EGFP at 250 μM and sodium fluorescein (46940, Sigma-Aldrich, St. Louis, MO) at 5% (w/v). Following injection, worms were mounted on an agarose pad in a drop of levamisole (0.25 mM in M9) for imaging. The time between injection and imaging was ~3 minutes.

For experiments requiring injection with both a dextran and a DNA stain, gonadal arms were first injected with 5 mg/mL Hoechst 33342 (B2261, Sigma-Aldrich, St. Louis, MO) in the middle of the MZ (estimated by the distance from the distal end of the gonad) followed by dextran injection.

Oil injections were performed with ES cell grade light mineral oil (ES-005-C, Millipore, Billerica, MA). Oil and injection capillaries were warmed to 65°C to facilitate needle filling, and cooled to room temperature prior to injection.

When temperature-sensitive strains were used, worms were kept in an incubator at the required temperature next to the injection set-up. One worm was removed at a time for injection. Following injection, worms were analyzed or moved to the desired temperature within 1 minute.

Statistics

The Wilcoxon rank sum test as implemented by the R-project was used for pairwise comparisons and confidence interval computation.

Supplementary Material

Refer to Web version on PubMed Central for supplementary material.

Acknowledgments

This work was supported by National Institutes of Health grants P50-GM076516, R21-AG042125, R01-GM102635, T32-EB009418, T32-HD060555, T15-LM007443, R01-GM107264 and R01-GM67247, and by National Science Foundation grant DMS 1161621 (Q.N.). Some strains were provided by the CGC, funded by NIH Office of Research Infrastructure Programs grant P40-OD010440. We are grateful to Peter Donovan for the loan of equipment, to Shaohua Zhou, Theodore Hazlett, Michelle Digman, and Enrico Gratton for providing facilities and technical assistance for FCS experiments, to UCI's Optical Biology Core Facility (supported in part by Cancer Center support grant CA-62203) for access to confocal microscopes, to Felix Grün for providing purified EGFP, and to Tim Schedl, Judith Kimble and Mihail Sarov for providing *C. elegans* strains.

References

Abi-Rached M, Brun J. Etude ultrastructurale des relations entre ovocytes et rachis au cours de l'ovogenèse du nématode Caenorhabditis elegans. Nematologica. 1975; 21:151–162.

Amini R, Goupil E, Labella S, Zetka M, Maddox AS, Labbé JC, Chartier NT. C. elegans Anillin proteins regulate intercellular bridge stability and germline syncytial organization. J Cell Biol. 2014; 206:129–143. [PubMed: 24982432]

Austin J, Kimble J. glp-1 is required in the germ line for regulation of the decision between mitosis and meiosis in C. elegans. Cell. 1987; 51:589–599. [PubMed: 3677168]

Brenner S. The genetics of Caenorhabditis elegans. Genetics. 1974; 77:71–94. [PubMed: 4366476]

Brunet I, Di Nardo AA, Sonnier L, Beurdeley M, Prochiantz A. The topological role of homeoproteins in the developing central nervous system. Trends Neurosci. 2007; 30:260–267. [PubMed: 17418905]

Byrd DT, Knobel K, Affeldt K, Crittenden SL, Kimble J. A DTC niche plexus surrounds the germline stem cell pool in Caenorhabditis elegans. PLoS ONE. 2014; 9:e88372. [PubMed: 24586318]

Chiang M, Cinquin A, Paz A, Meeds E, Price CA, Welling M, Cinquin O. Control of C. elegans germline stem cell cycling speed meets requirements of design to minimize mutation accumulation. BMC Biol. 2015; 13:51. [PubMed: 26187634]

Cinquin O, Crittenden SL, Morgan DE, Kimble J. Progression from a stem cell-like state to early differentiation in the C. elegans germ line. Proc Natl Acad Sci U S A. 2010; 107:2048–2053. [PubMed: 20080700]

Coppey, Berezhkovskii, Kim, Boettiger, Shvartsman. Modeling the bicoid gradient: Diffusion and reversible nuclear trapping of a stable protein. Dev Biol. 2007

Crittenden SL, Kimble J. Confocal methods for Caenorhabditis elegans. Methods Mol Biol. 1999; 122:141–151. [PubMed: 10231789]

Crittenden SL, Troemel ER, Evans TC, Kimble J. GLP-1 is localized to the mitotic region of the C. elegans germ line. Development. 1994; 120:2901–2911. [PubMed: 7607080]

Crittenden SL, Bernstein DS, Bachorik JL, Thompson BE, Gallegos M, Petcherski AG, Moulder G, Barstead R, Wickens M, Kimble J. A conserved RNA-binding protein controls germline stem cells in Caenorhabditis elegans. Nature. 2002; 417:660–663. [PubMed: 12050669]

Crittenden SL, Leonhard KA, Byrd DT, Kimble J. Cellular analyses of the mitotic region in the Caenorhabditis elegans adult germ line. Mol Biol Cell. 2006; 17:3051–3061. [PubMed: 16672375]

Dalfó D, Michaelson D, Hubbard EJA. Sensory regulation of the C. elegans germline through TGF-β-dependent signaling in the niche. Curr Biol. 2012; 22:712–719. [PubMed: 22483938]

Daniels BR, Rikhy R, Renz M, Dobrowsky TM, Lippincott-Schwartz J. Multiscale diffusion in the mitotic Drosophila melanogaster syncytial blastoderm. Proc Natl Acad Sci U S A. 2012; 109:8588–8593. [PubMed: 22592793]

Eckmann CR, Crittenden SL, Suh N, Kimble J. GLD-3 and control of the mitosis/meiosis decision in the germline of Caenorhabditis elegans. Genetics. 2004; 168:147–160. [PubMed: 15454534]

Eldar A, Rosin D, Shilo BZ, Barkai N. Self-enhanced ligand degradation underlies robustness of morphogen gradients. Dev Cell. 2003; 5:635–646. [PubMed: 14536064]

Fitzgerald K, Greenwald I. Interchangeability of Caenorhabditis elegans DSL proteins and intrinsic signalling activity of their extracellular domains in vivo. Development. 1995; 121:4275–4282. [PubMed: 8575327]

Fox PM, Vought VE, Hanazawa M, Lee MH, Maine EM, Schedl T. Cyclin E and CDK-2 regulate proliferative cell fate and cell cycle progression in the C. elegans germline. Development. 2011; 138:2223–2234. [PubMed: 21558371]

Francis R, Barton MK, Kimble J, Schedl T. gld-1, a tumor suppressor gene required for oocyte development in Caenorhabditis elegans. Genetics. 1995a; 139:579–606. [PubMed: 7713419]

Francis R, Maine E, Schedl T. Analysis of the multiple roles of gld-1 in germline development: interactions with the sex determination cascade and the glp-1 signaling pathway. Genetics. 1995b; 139:607–630. [PubMed: 7713420]

Frescas D, Mavrakis M, Lorenz H, DeLotto R, Lippincott-Schwartz J. The secretory membrane system in the Drosophila syncytial blastoderm embryo exists as functionally compartmentalized units around individual nuclei. J Cell Biol. 2006; 173:219–230. [PubMed: 16636144]

Furuta T, Tuck S, Kirchner J, Koch B, Auty R, Kitagawa R, Rose AM, Greenstein D. EMB-30: an APC4 homologue required for metaphase-to-anaphase transitions during meiosis and mitosis in Caenorhabditis elegans. Mol Biol Cell. 2000; 11:1401–1419. [PubMed: 10749938]

Gladfelter AS, Hungerbuehler AK, Philippsen P. Asynchronous nuclear division cycles in multinucleated cells. J Cell Biol. 2006; 172:347–362. [PubMed: 16449188]

Gregor T, Tank DW, Wieschaus EF, Bialek W. Probing the limits to positional information. Cell. 2007; 130:153–164. [PubMed: 17632062]

Guentchev M, McKay RDG. Notch controls proliferation and differentiation of stem cells in a dose-dependent manner. Eur J Neurosci. 2006; 23:2289–2296. [PubMed: 16706837]

Guruharsha KG, Kankel MW, Artavanis-Tsakonas S. The Notch signalling system: recent insights into the complexity of a conserved pathway. Nat Rev Genet. 2012; 13:654–666. [PubMed: 22868267]

Hall DH, Winfrey VP, Blaeuer G, Hoffman LH, Furuta T, Rose KL, Hobert O, Greenstein D. Ultrastructural features of the adult hermaphrodite gonad of Caenorhabditis elegans: relations between the germ line and soma. Dev Biol. 1999; 212:101–123. [PubMed: 10419689]

Hansen D, Schedl T. Stem cell proliferation versus meiotic fate decision in Caenorhabditis elegans. Adv Exp Med Biol. 2013; 757:71–99. [PubMed: 22872475]

Hansen D, Wilson-Berry L, Dang T, Schedl T. Control of the proliferation versus meiotic development decision in the C. elegans germline through regulation of GLD-1 protein accumulation. Development. 2004; 131:93–104. [PubMed: 14660440]

Hirsh D, Oppenheim D, Klass M. Development of the reproductive system of Caenorhabditis elegans. Dev Biol. 1976; 49:200–219. [PubMed: 943344]

Hopkins BD, Fine B, Steinbach N, Dendy M, Rapp Z, Shaw J, Pappas K, Yu JS, Hodakoski C, Mense S, et al. A secreted PTEN phosphatase that enters cells to alter signaling and survival. Science. 2013; 341:399–402. [PubMed: 23744781]

Hubbard EJA, Greenstein D. Introduction to the germ line. WormBook : the Online Review of C Elegans Biology. 2005:1–4. [PubMed: 18050415]

Kavousanakis ME, Kanodia JS, Kim Y, Kevrekidis IG, Shvartsman SY. A compartmental model for the bicoid gradient. Dev Biol. 2010; 345:12–17. [PubMed: 20580703]

Kershner AM, Shin H, Hansen TJ, Kimble J. Discovery of two GLP-1/Notch target genes that account for the role of GLP-1/Notch signaling in stem cell maintenance. Proc Natl Acad Sci U S A. 2014; 111:3739–3744. [PubMed: 24567412]

Kimble J. Alterations in cell lineage following laser ablation of cells in the somatic gonad of Caenorhabditis elegans. Dev Biol. 1981; 87:286–300. [PubMed: 7286433]

Kimble JE, White JG. On the control of germ cell development in Caenorhabditis elegans. Dev Biol. 1981; 81:208–219. [PubMed: 7202837]

Kimble J, Crittenden SL. Controls of germline stem cells, entry into meiosis, and the sperm/oocyte decision in Caenorhabditis elegans. Annu Rev Cell Dev Biol. 2007; 23:405–433. [PubMed: 17506698]

Kornberg TB, Guha A. Understanding morphogen gradients: a problem of dispersion and containment. Curr Opin Genet Dev. 2007; 17:264–271. [PubMed: 17643982]

Krejcí A, Bernard F, Housden BE, Collins S, Bray SJ. Direct response to notch activation: signaling crosstalk and incoherent logic. Science Signaling. 2009; 2:ra1. [PubMed: 19176515]

Lamont LB, Crittenden SL, Bernstein D, Wickens M, Kimble J. FBF-1 and FBF-2 regulate the size of the mitotic region in the C. elegans germline. Dev Cell. 2004; 7:697–707. [PubMed: 15525531]

Lander AD. Pattern, growth, and control. Cell. 2011; 144:955–969. [PubMed: 21414486]

Lander AD. How cells know where they are. Science. 2013; 339:923–927. [PubMed: 23430648]

Lander AD, Lo WC, Nie Q, Wan FYM. The measure of success: constraints, objectives, and tradeoffs in morphogen-mediated patterning. Cold Spring Harbor Perspectives in Biology. 2009; 1:a002022. [PubMed: 20066078]

Mavrakis M, Rikhy R, Lippincott-Schwartz J. Cells within a cell: Insights into cellular architecture and polarization from the organization of the early fly embryo. Communicative & Integrative Biology. 2009; 2:313–314. [PubMed: 19721875]

Mazzone M, Selfors LM, Albeck J, Overholtzer M, Sale S, Carroll DL, Pandya D, Lu Y, Mills GB, Aster JC, et al. Dose-dependent induction of distinct phenotypic responses to Notch pathway activation in mammary epithelial cells. Proc Natl Acad Sci U S A. 2010; 107:5012–5017. [PubMed: 20194747]

McGovern M, Voutev R, Maciejowski J, Corsi AK, Hubbard EJA. A “latent niche” mechanism for tumor initiation. Proc Natl Acad Sci U S A. 2009; 106:11617–11622. [PubMed: 19564624]

Morgan DE, Crittenden SL, Kimble J. The C. elegans adult male germline: stem cells and sexual dimorphism. Dev Biol. 2010; 346:204–214. [PubMed: 20659446]

Nadarajan S, Govindan JA, McGovern M, Hubbard EJA, Greenstein D. MSP and GLP-1/Notch signaling coordinately regulate actomyosin-dependent cytoplasmic streaming and oocyte growth in C. elegans. Development. 2009; 136:2223–2234. [PubMed: 19502484]

Nance J. C. elegans PAR-3 and PAR-6 are required for apicobasal asymmetries associated with cell adhesion and gastrulation. Development. 2003; 130:5339–5350. [PubMed: 13129846]

Ohlstein B, Spradling A. Multipotent Drosophila intestinal stem cells specify daughter cell fates by differential notch signaling. Science. 2007; 315:988–992. [PubMed: 17303754]

Ries J, Schwille P. Fluorescence correlation spectroscopy. BioEssays. 2012; 34:361–368. [PubMed: 22415816]

Rinne PL, van der Schoot C. Symplasmic fields in the tunica of the shoot apical meristem coordinate morphogenetic events. Development. 1998; 125:1477–1485. [PubMed: 9502728]

Sample C, Shvartsman SY. Multiscale modeling of diffusion in the early Drosophila embryo. Proc Natl Acad Sci U S A. 2010; 107:10092–10096. [PubMed: 20479267]

Sarov M, Murray JI, Schanze K, Pozniakovski A, Niu W, Angermann K, Hasse S, Rupprecht M, Vinis E, Tinney M, et al. A Genome-Scale Resource for In Vivo Tag-Based Protein Function Exploration in C. elegans. Cell. 2012; 150:855–866. [PubMed: 22901814]

Schmid M, Küchler B, Eckmann CR. Two conserved regulatory cytoplasmic poly(A) polymerases, GLD-4 and GLD-2, regulate meiotic progression in C. elegans. Genes Dev. 2009; 23:824–836. [PubMed: 19339688]

Schumacher B, Hanazawa M, Lee MH, Nayak S, Volkmann K, Hofmann ER, Hofmann R, Hengartner M, Schedl T, Gartner A. Translational repression of C. elegans p53 by GLD-1 regulates DNA damage-induced apoptosis. Cell. 2005; 120:357–368. [PubMed: 15707894]

Shestopalov VI, Bassnett S. Development of a macromolecular diffusion pathway in the lens. J Cell Sci. 2003; 116:4191–4199. [PubMed: 12953070]

Shi Y, Barton K, De Maria A, Petrash JM, Shiels A, Bassnett S. The stratified syncytium of the vertebrate lens. J Cell Sci. 2009; 122:1607–1615. [PubMed: 19401333]

Wolke U, Jezuit EA, Priess JR. Actin-dependent cytoplasmic streaming in C. elegans oogenesis. Development. 2007; 134:2227–2236. [PubMed: 17507392]

Wolpert L. One hundred years of positional information. Trends Genet. 1996; 12:359–364. [PubMed: 8855666]

Wong BG, Paz A, Corrado MA, Ramos BR, Cinquin A, Cinquin O, Hui EE. Live imaging reveals active infiltration of mitotic zone by its stem cell niche. Integr Biol. 2013; 5:976–982.

Yan D, Wu Y, Yang Y, Belenkaya TY, Tang X, Lin X. The cell-surface proteins Dally-like and Ihog differentially regulate Hedgehog signaling strength and range during development. Development. 2010; 137:2033–2044. [PubMed: 20501592]

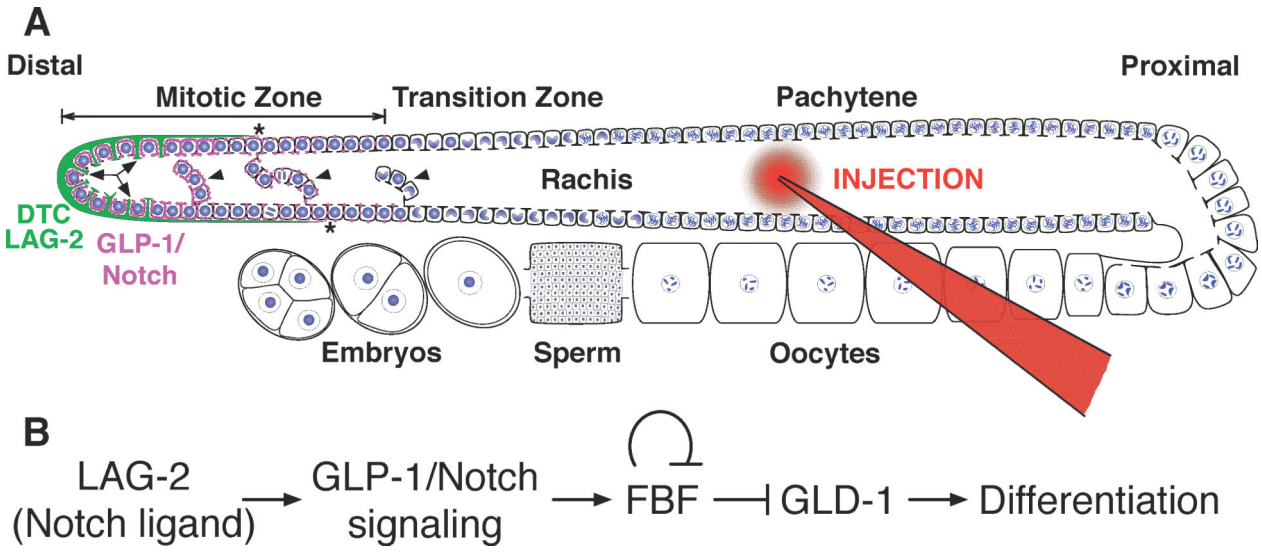

Figure 1.

Gonadal arm organization and core regulatory network controlling differentiation.

(**A**) *C. elegans* hermaphrodite gonadal arms comprise a Mitotic Zone (MZ) at the distal end; stem cells are maintained by a niche formed by the distal tip cell (DTC; green), which supplies ligands including LAG-2 that activate the GLP-1/Notch receptor in germ cells and thereby maintain the MZ. The DTC forms tight contact with distal germ cells (arrows) and also extends long, thin processes (ends marked by asterisks). Germ cells are displaced from the distal end to the proximal end as they differentiate and progress through meiosis. The rachis, a central core in the gonadal arm, provides a connection between the cytoplasm of individual germ “cells”, which thus form a syncytium. Distally, cell bridges partially span the rachis (arrow heads). Schematic red needle shows approximate site of proximal rachis injections in experiments described below.

(**B**) Core regulatory network used in simulations. Notch signaling promotes expression of FBF, which represses itself and GLD-1. Differentiation (i.e. meiotic entry) is assumed to occur when GLD-1 reaches a critical threshold.

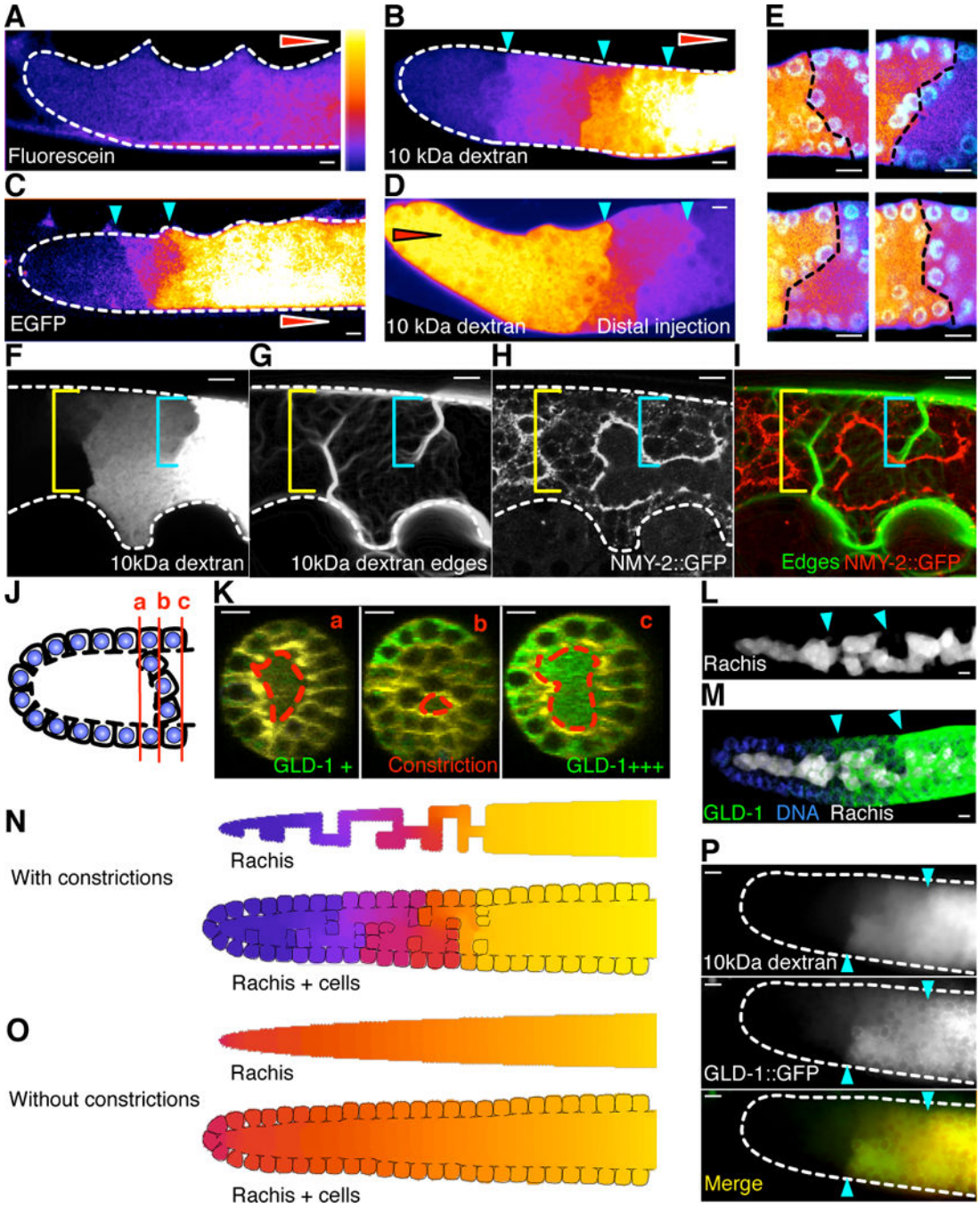

Figure 2.

Long-range diffusion diffusion in the germline is impeded by semi-permeable barriers. (**A – D**) Distribution along the distal-proximal axis of proximally-injected fluorescein (**A**), EGFP (B) and 10 kDa dextran (**C**); steps in intensity (cyan arrowheads) reveal diffusion barriers. Diffusion barriers are also apparent following distal injection of dextran (**D**). Fluorescence intensity is color-coded using a “fire” lookup table (range displayed on right of fluorescein injection), and injection sites are marked by red arrowheads.

(**E**) Injected dextran steps colocalize with cell bridges (Hoechst-stained nuclei overlaid in cyan; 4 steps are shown that occurred in the same gonadal arm).
(**F – I**) Steps in injected dextran colocalize with cell bridges. Dextran fluorescence signal (**F**) was processed by an edge-enhancing image filter (**G**), and compared with the membrane marker NMY-2::GFP (**H**; overlay: **I**). Cyan and yellow bars shown step positions.
(**J – K**) Transverse MZ sections (**J**) show lower GLD-1 levels (green) just distal to a cell bridge (position 'a') compared to just proximal (position 'c'; **K**). The rachis (dashed red line in transverse sections) is constricted at the position the cell bridge occurs (position 'b'). Cell membranes are highlighted by Phalloidin staining (yellow).
(**L – M**) 3D opacity rendering of rachis (**L**) overlaid with DNA and GLD-1 (blue and green, respectively; **M**) similarly shows GLD-1 steps (cyan arrowheads) co-localizing with rachis constrictions.
(**N – O**) Simple two-dimensional diffusion model accounts for creation of injected dextran steps by rachis constrictions. Diffusion of proximally-injected dextran with a coefficient of 20 $\mu m^2.s^{-1}$ over a period of 30 minutes was simulated either with (**N**) or without (**O**) local constrictions in the rachis. Simulated dextran concentration is coded using a "Fire" lookup table as in (**A**) above. Simulations were performed by collapsing cells into an infinitely-thin layer. The result of each simulation is displayed with or without cells present around the rachis.
(**P**) Steps in intensity of proximally-injected 10 kDa dextran (top; cyan arrowheads) co-localize with steps in endogenous GLD-1::GFP (middle) as shown in color overlay (bottom). Scale bars: 5 μm.

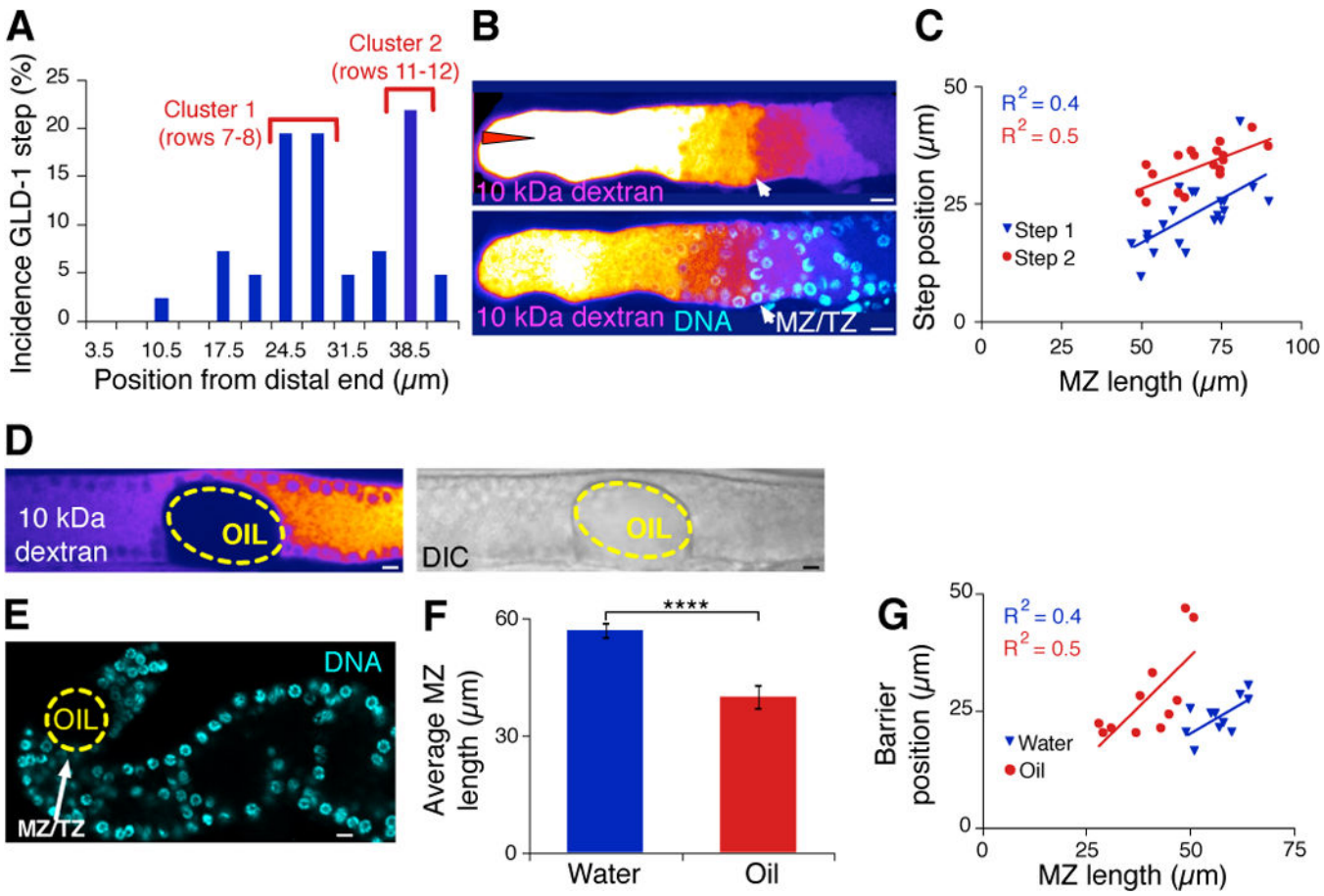

Figure 3.

Sites of diffusion barriers are clustered and correlate with MZ length.

(**A**) Two GLD-1 steps are commonly found that cluster at positions ~24–28 μm (rows 7–8) and ~38 μm (rows 11–12).

(**B**) Diffusion barrier observed at the MZ/TZ boundary (white arrow; n = 10). Top panel uses enhanced contrast ("Fire" look-up table) to show weak proximal signal of 10 kDa dextran injected distally (red arrowhead); bottom panel shows overlay with DNA (cyan).

(**C**) Correlation between positions of GLD-1 steps and MZ length. Step 1 is the most distal step.

(**D – G**) Artificial barriers correlate with and control MZ length. Oil droplet injection in the pachytene region creates a diffusion barrier revealed by subsequent injection of 10 kDa dextran (**D**; the distal end, not in sight because the droplet is in the proximal pachytene region, is to the left). Distal oil droplets reduce MZ length compared to water injected controls (**E – F**; $p < 1.8E-05$); artificial and endogenous diffusion barrier positions correlate with MZ length with similar R^2 values (**G**).

Scale bars: 5 μm.

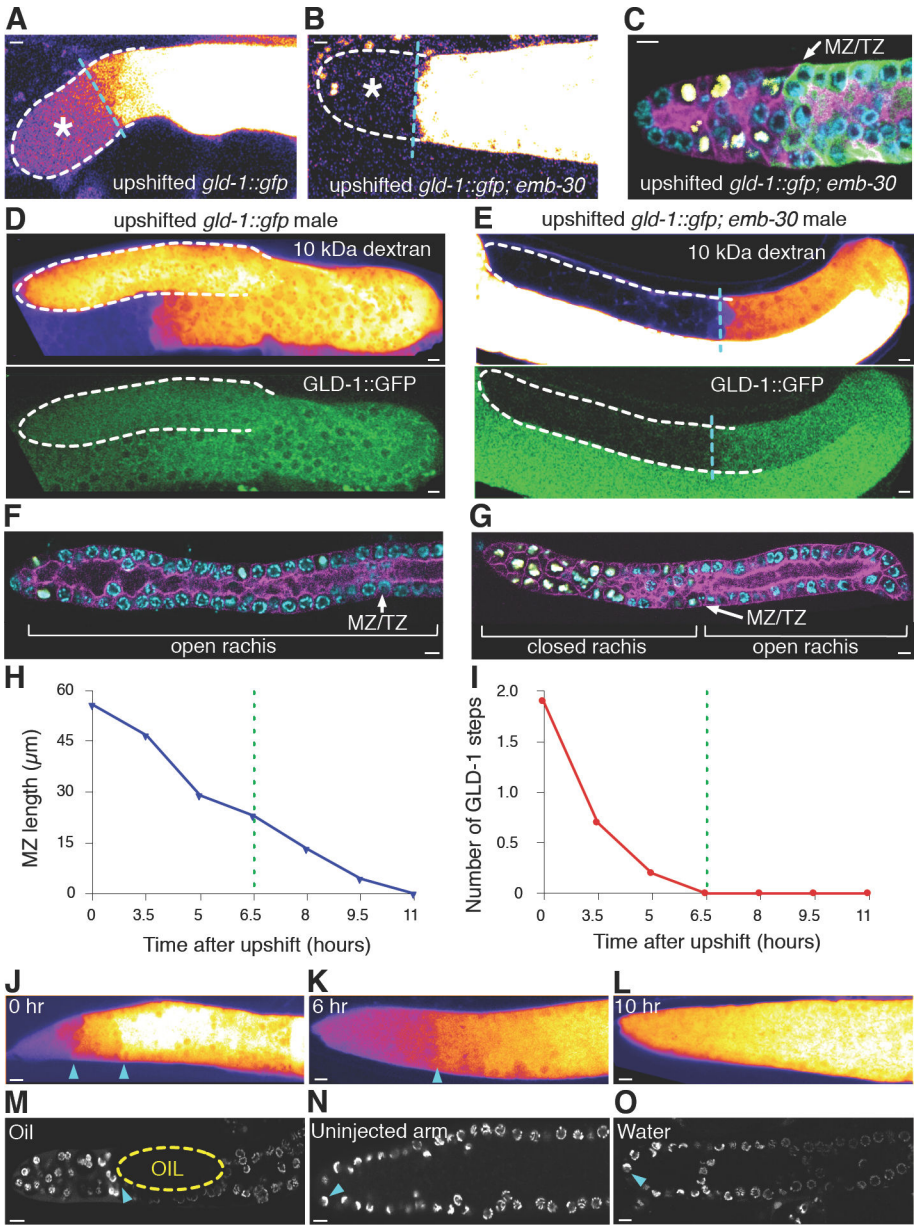

Figure 4.

(**A – G**) Upshift of *emb-30(ts)* mutant results in a 10 kDa dextran-impermeable barrier between undifferentiated and differentiated cells.

(**A – C**) The distal-most region in upshifted *gld-1::gfp* controls accumulates low levels of proximally-injected dextran (**A**; asterisk) whereas in upshifted *gld-1::gfp; emb-30* no dextran is detected distally (**B**; contrast enhanced to show absence of detectable distal signal). The rachis is closed off by cell membranes at the MZ/TZ (arrow in **C**) in upshifted *gld-1::gfp; emb-30*. GLD-1::GFP: green; membrane: magenta; M-phase cells: yellow; DNA: cyan.

(**D – E**) Distal diffusion of injected dextran occurs freely in upshifted *gld-1::gfp* control males (**D**); however a *de novo* diffusion barrier (cyan dotted line) is formed in upshifted *gld-1::gfp; emb-30* males (**E**).
(**F – G**) The rachis remains unobstructed in upshifted controls (**F**) but becomes sealed distally at the MZ/TZ boundary in upshifted *gld-1::gfp; emb-30* males (**G**). Membrane: magenta, M-phase cells: yellow, DNA: cyan.
(**H – O**) Barriers can protect the MZ from pro-differentiation factors. Following *glp-1* upshift distal cell differentiation occurs and mitotic zone length reaches 0 (**H**), which is preceded by the disappearance of steps in GLD-1 (**I**). Diffusion barriers revealed by dextran injection similarly disappear in response to *glp-1* upshift: at 0 hr two barriers are present (**J**; cyan arrowheads), by 6.5 hr only one weak barrier is visible (**K**), and by 10 hr no diffusion barriers are observed (**L**). Artificial barriers formed by injection of an oil droplet block germ cell differentiation up to 18 hr after *glp-1* upshift (**M**); uninjected gonadal arms belonging to specimens whose other arm was injected with oil (**N**) or injected with water (**O**) differentiate normally, as shown by crescent-like morphology of distal-most cells (arrowheads). MZ length after oil injection and 18 hr upshift is ~27 μm (n = 9), significantly higher than control MZ length, which is 0 (n = 6 for uninjected arms, n = 10 for water-injected arms, $p < 3E-3$ and $p < 5E-4$, respectively).
Scale bars: 5 μm.

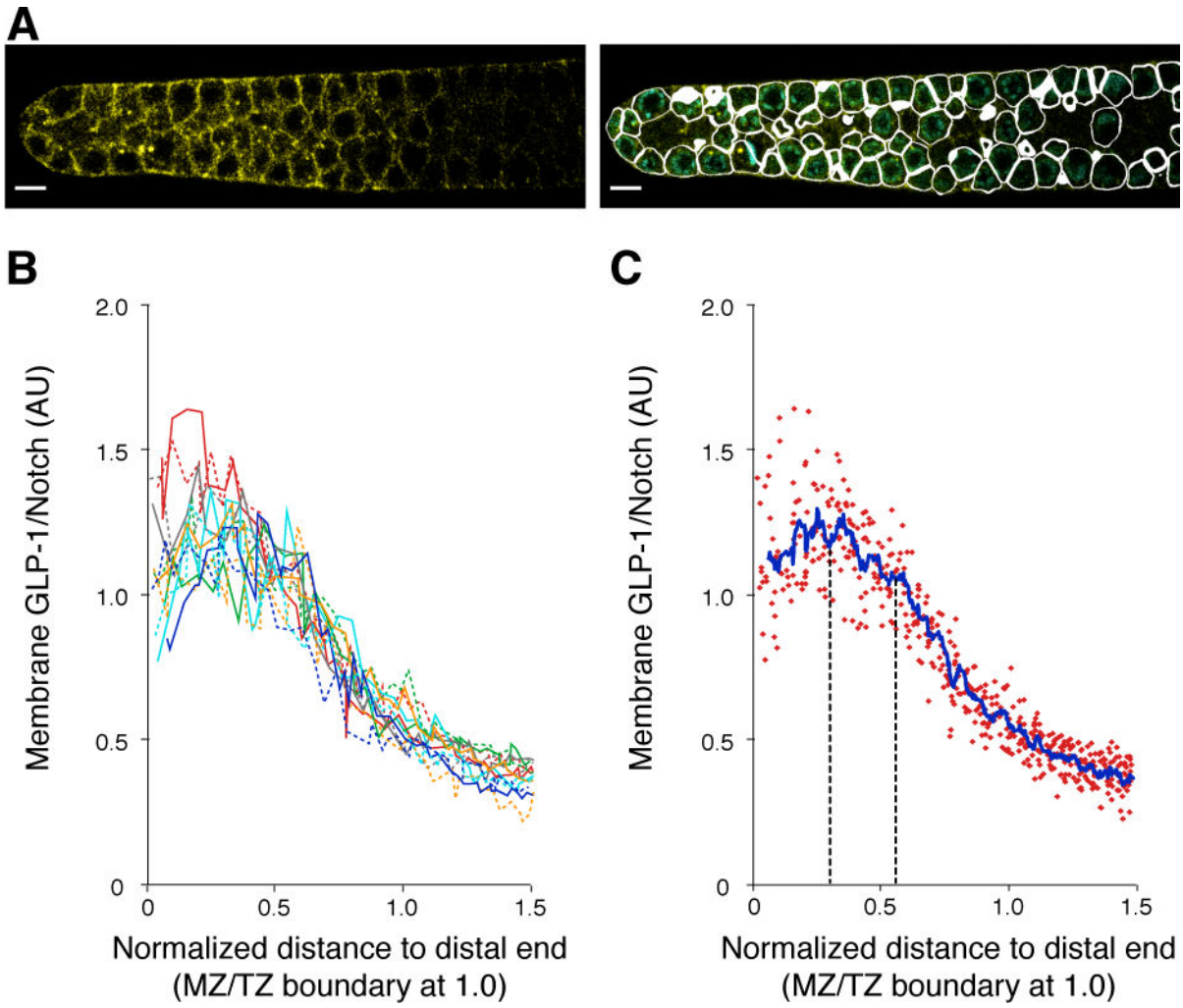

Figure 5.

Notch is expressed at a high level in the distal half of the mitotic zone, and shows a noisy spatial distribution.

(**A**) Notch (yellow) is predominantly localized to plasma membrane that tightly encloses nuclei, and is expressed in a gradient in the proximal MZ. Left panel shows Notch staining, while right panel shows an overlay of Notch, DNA (cyan), and active contour segmentations used for quantification shown in other panels (white). Scale bars: 5 μm.

(**B**) Overlay of membrane GLP-1::GFP profiles quantified from 12 different gonads.

(**C**) Membrane GLP-1::GFP profile (blue line) computed as a moving average of cells pooled from same 12 gonads as shown in (B). Each dot represents one cell. Dotted lines show positions of the diffusion barrier clusters identified in Figure 3A.

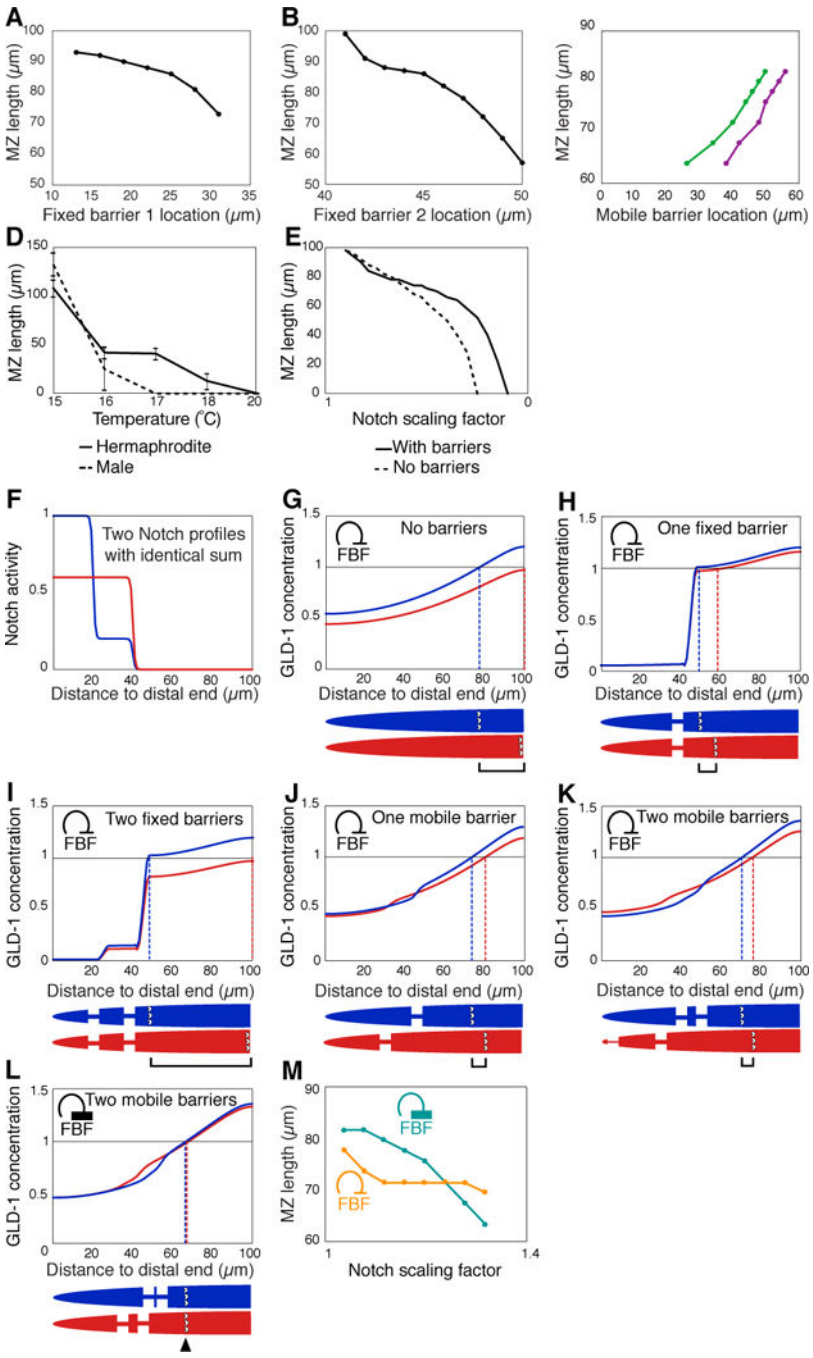

Figure 6.

Mobile diffusion barriers correlate positively with MZ length and provide robustness against fluctuations in the spatial distribution of Notch signaling.

(**A—C**) Following a model by which MZ size is set by a threshold level of 1.0 arbitrary GLD-1 units and by which two fixed diffusion barriers slow down GLD-1 and FBF diffusion (see main text), barrier distance to the distal end correlates negatively with MZ size as total Notch signaling intensity is scaled (A: correlation with distal-most barrier in a two-barrier system; B: correlation with proximal-most barrier; simulation parameters given

in Data S1 Table 2). By contrast, correlation between position of mobile barriers and MZ size is positive (**C**; plotted with FBF self-repression coefficient $\beta_F = 1$ to allow for realistic barrier positioning).

(**D**) MZ length of the *glp-1(q224)* Notch mutant, measured at L4 + 1 day in males and hermaphrodites grown at the indicated temperature from the L1 stage (0 indicates absence of MZ).

(**E**) MZ length determined from computational simulations of model with mobile barriers, as a function of Notch scaling factor (1: full Notch activity; 0: no Notch).

(**F—G**) Two spatial Notch activity profiles that sum to the same value but differ in shapes (**F**, red and blue curves) lead to substantially different GLD-1 profiles and MZ sizes if no barriers are present (**G**). Bracket shows the difference in MZ size between the two simulations (MZ/TZ boundary shown by crescent-shaped nuclei).

(**H—I**) One fixed diffusion barrier can largely prevent the change in GLD-1 profiles and in MZ size (F), while two fixed barriers can paradoxically increase the change in MZ size (G).

(**J—K**) Mobile barriers, whose positions are dynamically updated to follow threshold GLD-1 values, provide robustness of MZ size against spatial fluctuations in Notch whether a gonadal arm has a single barrier (**J**) or two (**K**).

(**L—M**) Stronger FBF self negative feedback increases robustness of MZ size to the spatial distribution of Notch (**L**), but moderately decreases robustness to changes in total Notch (**M**).